25. Harada, T. *et al.* Visualization of volatile substances in different organelles with an atmospheric-pressure mass microscope. *Anal Chem.* **81**, 9153–9157 (2009).

## Acknowledgments

This work was supported by the Funding Program for World-Leading Innovative R&D on Science and Technology (FIRST Program) (YM), Third Term Comprehensive Control Research for Cancer from the Ministry of Health, Labour and Welfare of Japan (YM), a Grant-in-Aid for Scientific Research on Priority Areas from the Ministry of Education, Culture, Sports, Science and Technology, the National Cancer Center Research and Development Fund (YM and MY), the Kobayashi Foundation Research Grant for Cancer Research (MY), and a Grant-in-Aid for Scientific Research from the Japan Society for the Promotion of Science (MY). We thank Mrs K. Shiina for her secretarial support.

## Author contributions

Y.M. developed the method. M.Y., M.F., K.O., Y.K., Y.Y. and M.T. performed the experiments and analysed the data. Y.M. and M.Y. wrote the manuscript.

## Additional information

**Competing financial interests:** The authors declare no competing financial interests.

**How to cite this article:** Yasunaga, M. *et al.* The significance of microscopic mass spectrometry with high resolution in the visualisation of drug distribution. *Sci. Rep.* **3**, 3050; DOI:10.1038/srep03050 (2013).

Microvascular Reviews and Communications



Vol.6 No.1

# Tumor stromal barrier and cancer stromal targeting therapy

Masahiro Yasunaga[1], Shino Manabe[2] and Yasuhiro Matsumura[1,*]
1) Division of Therapeutic Development, Research Center for Innovative Oncology, National Cancer Center Hospital East
2) Synthetic Cellular Chemistry Laboratory, RIKEN

## *Abstract*

Antibody drug conjugates (ADCs) are effective for tumors with no or little stroma, such as malignant lymphoma or breast cancer. However, in refractory cancers (pancreatic cancer or scirrhous gastric cancer) forming hypovascular and stroma-rich tumors, the penetration of monoclonal antibodies (mAbs) into the cells is impeded (stromal barrier), which leads to failure of conventional cell-targeting ADCs. To overcome this, we developed cancer stromal targeting (CAST) therapy using anti-collagen IV or anti-fibrin mAbs. These stroma-targeting ADCs selectively extravasated from leaky tumor vessels and bound to collagen IV or fibrin on the tumor stroma, from which effective sustained release of the payload drug occurred. The released drug subsequently diffused through the tumor tissue, causing marked arrest of tumor growth associated with damage to tumor vessels and death of cancer cells. In terms of the pathological findings after treatment, empty sleeves collagen IV-positive and CD31-negative remnant ring structures) were observed in the destroyed vessels. This review highlights the tumor stromal barrier and the development of CAST therapy. Insights into the pharmacokinetics and efficacy of antibodies or ADCs may also be informative to understand the pathophysiological role of the tumor microcirculation involved in the stromal barrier. [MVRC 6(1): 2-8, 2013]

**Key words:** cancer, stromal barrier, antibody, ADC, CAST

*Received 2013/5/20, Accepted 2013/9/2*
*To whom correspondence should be addressed: Dr. Yasuhiro Matsumura, Division of Therapeutic Development, Research Center for Innovative Oncology, National Cancer Center Hospital East, 6-5-1 Kashiwanoha, Kashiwa, Chiba 277-8577, Japan
E-mail: yhmatsum@east.ncc.go.jp

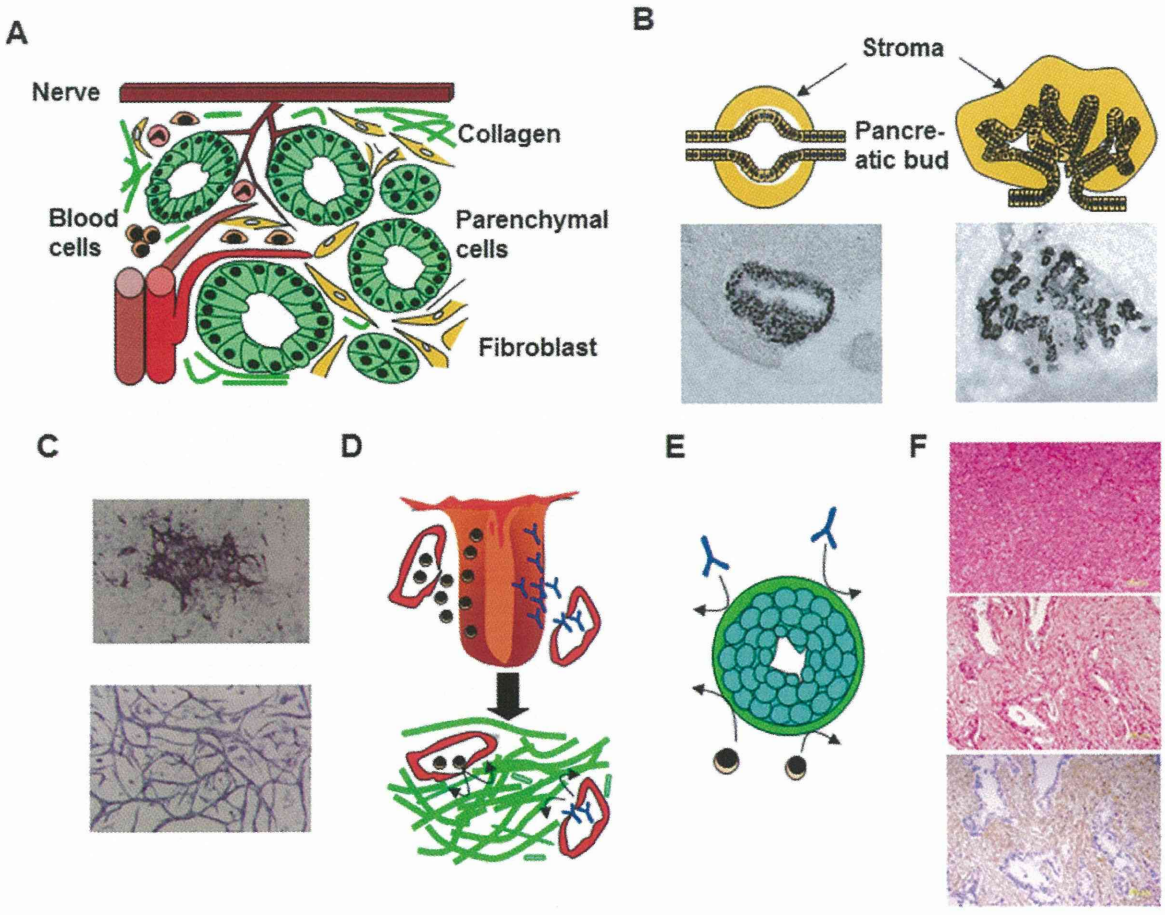


**Fig. 1.** Physiological and pathophysiological roles of stroma. (A) Parenchymal cells and stroma. (B) Pancreas organogenesis induced by stroma. (C) VEGF and collagen IV promote insufficient vasculogenesis (upper panel). Well-organized vascular tube formation occurred in the presence of stoma cells (lower panel). (D) Stroma suppresses overreaction of the inflammation. (E) Stroma defends the reproductive system against autoimmune attack. (F). Hematoxylin-eosin staining of malignant lymphoma (ML) (upper panel) and pancreatic cancer (PC) (middle panel). Immunostaining of stromal collagen IV (brown) in PC. Cancer cells were stained by eosin (blue) (lower panel).

## Introduction

Although many monoclonal antibodies (mAbs) have already been approved for the treatment of cancer, they are usually used in combination with anticancer agents (ACAs) because of their limited anti-tumor activity when used alone[1]. Antibody-drug conjugates (ADCs), the next generation of therapeutic antibodies, are a promising strategy to enhance the cytotoxic effect[2–4]. Conventional ADCs depend on enzymatic cleavage following internalization into the cytoplasm or lysosome. Most human solid tumors, however, possess abundant stroma, which hinders the distribution of ADCs (stromal barrier). Moreover, the process of cell uptake is disturbed by the stromal barrier. Therefore, this barrier limits the effectiveness of ADCs, regardless of the internalization ability. The heterogeneity of tumor cells also prevents the development of ADC therapy based on a cell-specific antigen[5–8].

To overcome these issues, we created a unique type of ADC, namely, cancer stromal targeting (CAST) therapy, in which stroma-targeting mAbs (anti-collagen IV or anti-fibrin mAbs) were conjugated to cytotoxic ACAs[6–8]. Our ADC bound to collagen IV or fibrin in the stroma, from which sustained release of ACAs and their distribution throughout the tumor occurred; this had a strong anti-tumor effect against stroma-rich tumors compared with that of conventional ADCs[5–8].

In this article, we initially outline the tumor stromal barrier and conventional ADCs, followed by an introduction and discussion of CAST therapy.

### Physiological and pathophysiological roles of stroma

Organ or tissue consists of not only parenchymal cells but also stroma. Stroma has various components such as fibroblasts, blood vessels, and nerve or extracellular matrix proteins, for example, collagen, fibrin and fibronectin (Fig. 1A). As a result, stroma exhibits various biological activities[9–12]. In embryogenesis, stroma can induce organogenesis of the pancreas, liver or lung (Fig. 1B). Regarding tissue remodeling, vasculogenesis by endothelial progenitors is promoted by collagen IV and VEGF, but the tube formation is insufficient, whereas well-organized vascular tube formation occurs in the presence of stroma cells (Fig. 1C). Upon inflammation, stroma blocks the overreaction of immune cells and terminates inflammatory process (Fig. 1D). Stroma also acts in host defense within the reproductive system (Fig. 1E).

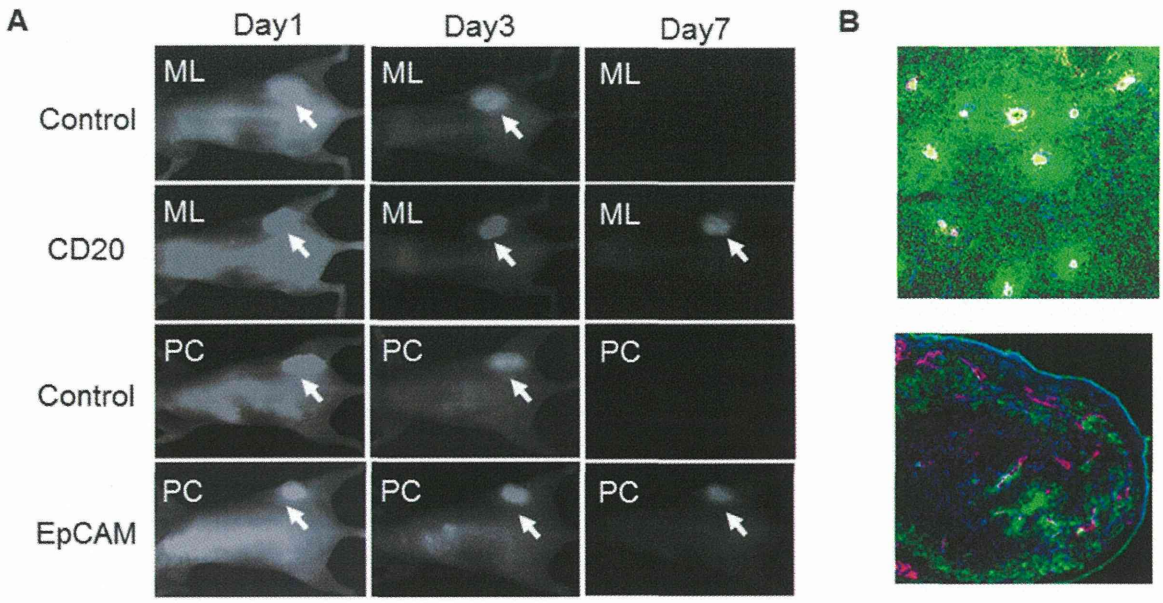


**Fig. 2.** Antibody delivery in malignant lymphoma and pancreatic cancer. (A) In vivo imaging of fluorescent mAbs. Anti-CD20 and anti-EpCAM mAbs were injected into malignant lymphoma (ML) and pancreatic cancer (PC) models, respectively. Non-specific mAb was used as a control. (B) Distribution of anti-CD20 mAb (green) and anti-EpCAM mAb (green) within ML tumor and PC tumor, respectively. Blood vessels (whitish-yellow in upper panel, magenta in lower panel) are shown.

In malignant tissues, stroma promotes the growth, survival, invasion or metastasis of tumor cells. It is thus increasingly important to understand the role of the stroma in tumorigenesis[13–17]. There are two distinct types of tumor tissue: those with little stroma, for example, malignant lymphoma (ML), and those with dense stroma, for example, pancreatic cancer (PC) (Fig. 1F), and the latter is strongly associated with the treatment-resistant phenotype.

**Antibody drug conjugate and stromal barrier**

Recently, several ADCs have been approved for oncological treatment[1–4]. These antibody therapies are effective for ML or breast cancer (BC), but not for refractory cancers such as PC or scirrhous gastric cancer (SGC). Although many researchers have investigated the molecular mechanism behind enhanced anti-apoptotic effect, the abundance of drug-efflux transporters or the existence of natural chemoresistant cancer stem cells, in order to solve this question, the issue of the tumor stromal barrier has been almost entirely overlooked. We speculated that dense stroma prevents antibody distribution within tumor tissue, which would be one of the reasons for therapeutic resistance. Therefore, in a previous study, we evaluated antibody using an in vivo imaging system. We used two types of tumor model: ML and PC. Anti-CD20 mAb and anti-EpCAM mAb were also used as specific mAbs against ML and PC, respectively. In whole body imaging, both non-specific mAbs and specific mAbs accumulated in the tumor by an enhanced permeability and retention (EPR) effect[18] as passive targeting on Day 3 after injection (Fig. 2A). High-molecular-weight agents including mAbs were shown to extravasate from leaky tumor vessels but not normal tissues[18]. Moreover, they remained at the site for a long time because of the lack of effective lymphatic drainage, which impeded the efficient clearance of mAbs accumulated in solid tumor tissues[18]. On Day 7, although non-specific mAbs disappeared from the tumor, specific mAbs still accumulated there by utilizing their specific antigen-binding ability (Fig. 2A). We considered mAbs to be one of the ideal drug delivery system (DDS) carriers because IgG ranging in size from 10 to 20 nm can utilize the EPR effect[18]. Moreover, specific mAbs were able to stay longer by the EPR effect plus active targeting.

We then examined the mAb distribution within tumor tissue. Extravasated anti-CD20 mAbs were distributed throughout the whole tumor in ML, whereas the distribution of anti-EpCAM mAbs was restricted to the tumor margin adjacent to vessels in PC. A very small amount of mAb reached the central area within the tumor (Fig. 2B). This phenomenon can be explained by the stromal barrier. Although some authors reported that mAbs extravasted from leaky tumor vessels were able to reach the tumor cells sufficiently, they used hypervascular and stroma-less tumor models[19, 20]. We therefore considered these models were close to the ML rather than PC. On the other hand, genetic engineered mouse (GEM) models have come to be used for the studying human cancer[21]. The pancreatic tumors observed in the model displayed pathophysiological features similar to human pancreatic cancers. By using this model, it was shown that the dense stromal was able to prevent drug delivery into the tumor cells[23, 24]. We speculate that stromal barrier involves three factors: 1) mechanical interference by stromal cells and extracellular proteins, 2) pharmacological disturbance depending on low convection and diffusion, and 3) a long distance from vessels to tumor cells. We need to further investigate the mechanism of the stromal barrier to elucidate this hypothesis.

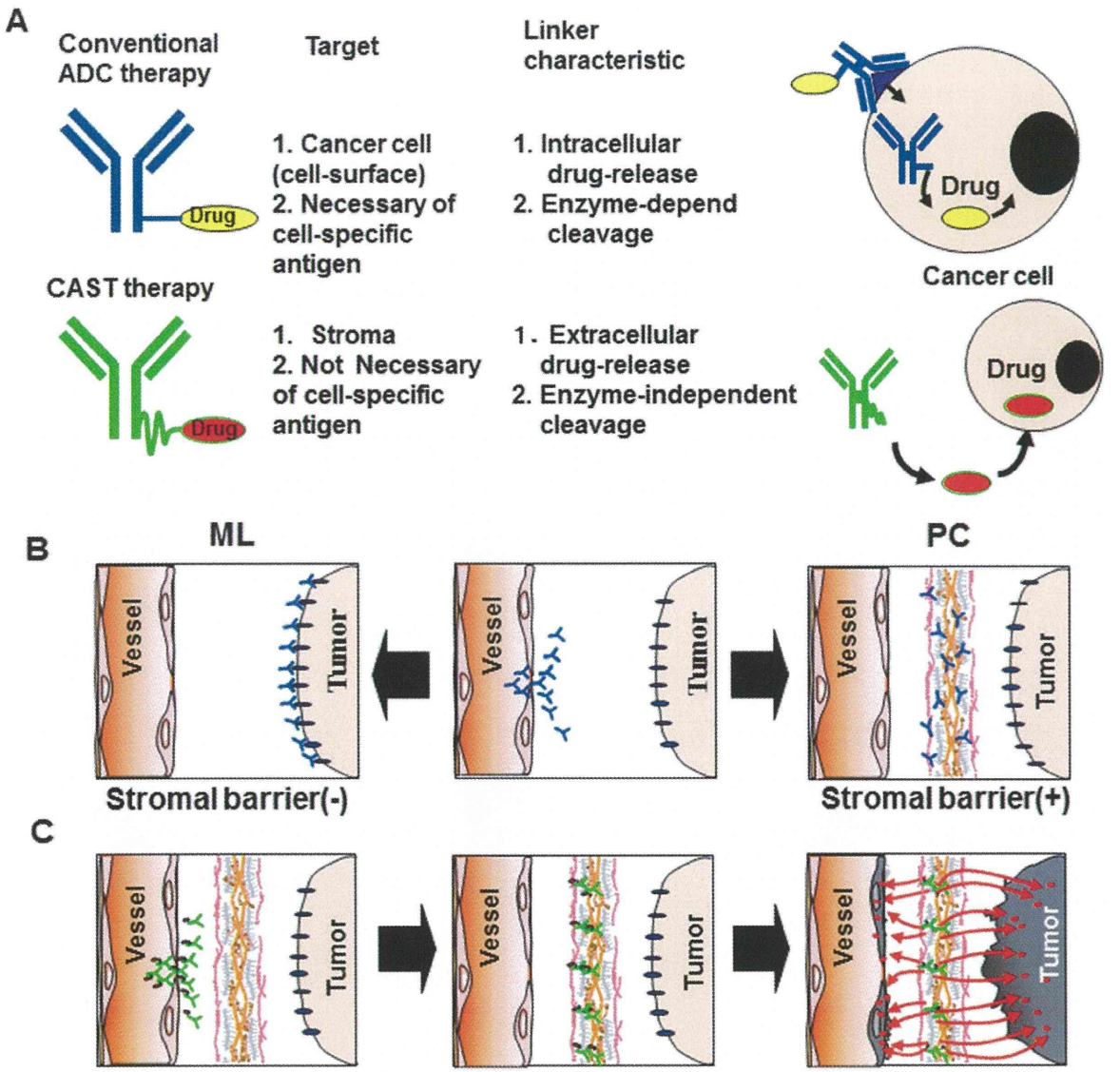


**Fig. 3.** Conventional ADC and CAST therapy. (A) Comparison between conventional ADC and CAST therapy. (B) Conventional ADC can be distributed and reach the tumor cell in the absence of a stromal barrier, but not in the presence of one. (C) CAST therapy ADC can accumulate on stroma, from which sustained release of the drug can occur and attack both tumor cells and tumor vasculature because a small molecule drug is not influenced by the stromal barrier.

**Conventional ADCs**

In the 1980s, the development of anti-tumor-cell-specific mAbs carrying a cytotoxic drug, known as missile therapy and expected to be a magic bullet for cancer treatment, was actively pursued. However, the induction of human anti-mouse antibody (HAMA) response was a major impediment to the success of antibody-related therapies. In addition, most of the linkers connecting the cytotoxic drug to an mAb were unstable and easily degraded in the body. Fortunately, recent progress in antibody engineering and linker technology has overcome these problems[1-4]. Chimeric or humanized mAb reduces the rate of HAMA reactions. In addition, linkers that are stable enough in the body to last until the ADC reaches the tumor cells, and also sufficiently cleavable to allow effective drug release within cells, have been successfully developed[2-3] (Fig. 3A and B). Recently, the clinical benefit of newly developed anti-HER2 mAb-DM1 has been demonstrated in the treatment of BC[4]. However, there is less stroma in BC than in refractory solid tumors such as PC or SGC. Moreover, most BCs are hypervascular tumors, in which the stromal barrier may be weakened. Furthermore, the treatment is limited to HER2-overexpressing tumors. Most human refractory solid tumors, however, possess hypovascularity and dense stroma that hinders the distribution of ADCs (Fig. 3B). ADCs can release drug by enzymatic cleavage after internalization into a cell and delivery to the lysosome. However, the stromal barrier in solid tumor prevents ADCs from reaching the cells. Unlike the limited cases of HER2-overexpressing BC, in most cases, heterogeneity of the tumor cells prevents the development of ADC therapy

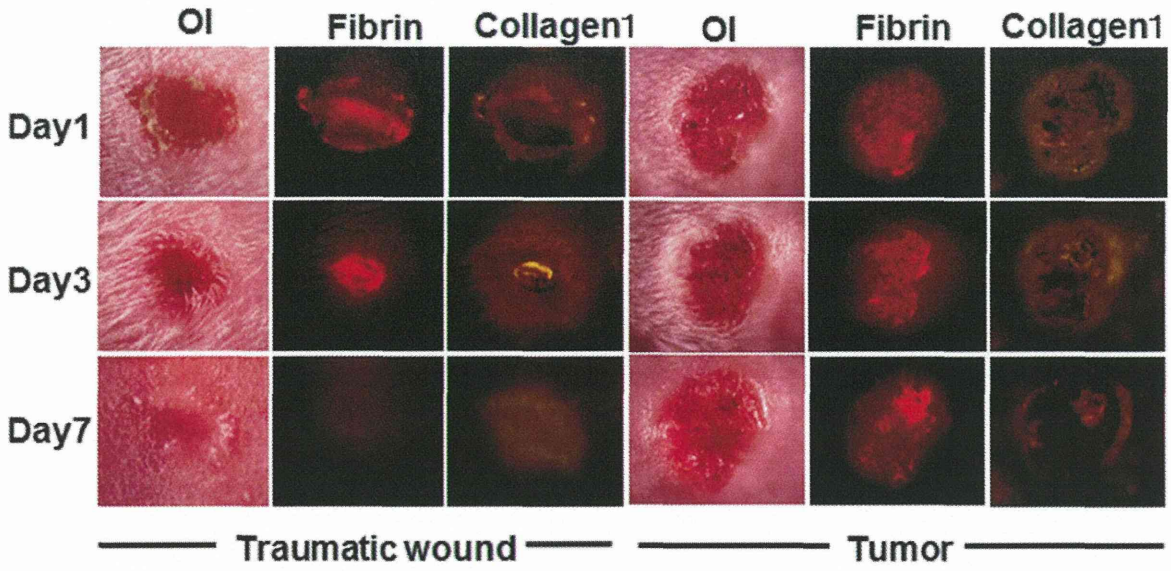


**Fig. 4.** Tumor specificity of anti-fibrin mAb. Biodistribution of Alexa 647-labeled anti-fibrin mAb (Red) and Alexa 555-labeled anti-collagen-1 mAb in mouse bearing a traumatic wound (left columns) and tumor (right columns) on days 1, 3 and 7 after the injection. OI: optical image.

based on a cell-specific antigen. It seems that conventional cell-targeting ADC therapy is effective for hematological malignancy (ML) or hypervascular solid tumors having little stroma (BC), but not for high-stromal hypovascular solid tumors (PC).

### CAST therapy

To overcome the limitations of conventional ADCs, we created CAST therapy, which utilizes abundant stroma as a scaffold for drug delivery (Fig. 3A and C). It was composed of ACAs conjugated to stroma (collagen IV or fibrin)-targeting mAb via an ester-bond linker[6–8]. Our stroma-targeting ADCs were shown to reach tumor passively by the EPR effect[18]. Moreover, they bound to the tumor stroma, from which effective sustained release of ACAs occurred. The released ACAs could be distributed throughout the tumor because the ester bond could gradually be cut by hydrolysis (non-enzymatically) outside of the cells. Polyethylene glycol (PEG) adjacent to the ester bond protected the degradation of the bond in the blood before the tumor was reached. ACAs released from the ADCs were shown to damage both tumor cells and tumor vessels, which resulted in the arrest of tumor growth[6–8]. We focused on two stromal components, fibrin and collagen, the levels of which are generally high in tumors. In non-malignant diseases such as cerebrovascular disease, cardiac infarction, traumatic wound and rheumatoid arthritis, fibrin formation occurs at onset or during the active phase. At 7 days after onset, fibrin disappears and is replaced by collagen. A contracted collagenous scar is then formed as the final step of healing. On the other hand, in malignant tumor, bleeding, fibrin formation and collagen replacement as a malignant cycle of blood coagulation are reproduced as long as tumor cells exist and invade the adjacent vasculature[5].

To confirm the specificity of fibrin clot formation, anti-fibrin-specific mAbs were administered to mouse bearing both tumor and traumatic wound. The anti-fibrin mAbs disap-

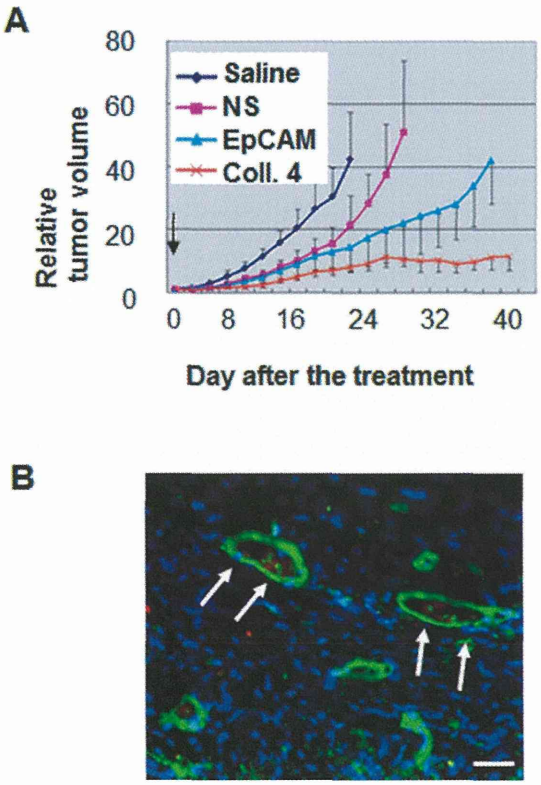


**Fig. 5.** Anti-collagen IV ADC. (A) Anti-tumor effect of anti-collagen IV ADC (Coll.4) was compared with control (saline), non-specific mAb ADC (NS) and anti-EpCAM ADC (EpCAM). SN-38 is used as the payload. (B) Damaged tumor vasculature immunostained by CD31 (red), collagen IV (green) and DAPI (blue) is shown. Arrow indicates CD31-negative, collagen IV-positive ring structure. Scale bar, 20 μm.

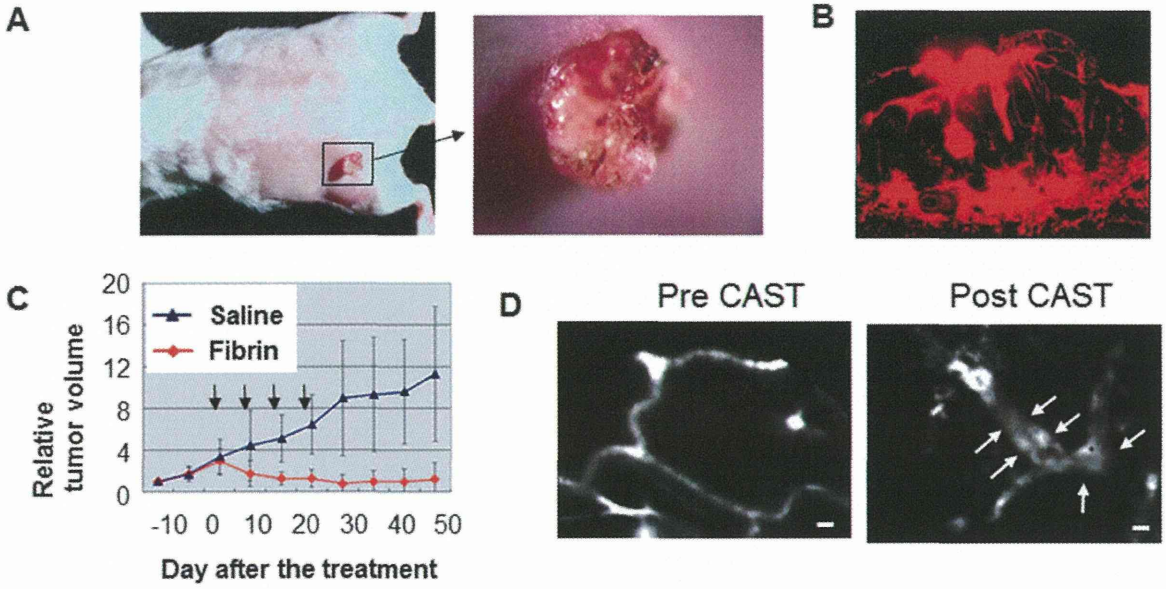


**Fig. 6.** Anti-fibrin ADC. (A) Chemically induced skin cancer model. (B) Immunostaining of fibrin (red). (C) Anti-tumor effect of anti-fibrin ADC is compared with control (saline). (D) Destroyed tumor vasculature (right column) is shown in comparison with pretreatment (left column). Scale bar, 10 μm.

peared from healing traumatic wound, whereas they still accumulated in the non-healing tumor (Fig. 4).

**Anti-tumor activity of CAST therapy**

We used a PC xenograft model to examine the anti-tumor effect of anti-collagen ADC compared with anti-CD20 ADC as non-specific targeting, anti-EpCAM ADC as specific cell targeting or saline as a control. Anti-collagen IV ADC exerted the most potent antitumor activity among them[7, 8] (Fig. 5A). Destroyed tumor vasculature that involved empty sleeves of basement membrane was observed[7, 8] (Fig. 5B). There was no hepatotoxicity, nephrotoxicity or bone marrow toxicity in the treated mice. In addition, no autoimmune disease-like adverse effects such as arthritis were observed upon the administration of anti-collagen IV mAb, whereas anti-collagen II mAb combined with lipopolysaccharide caused severe arthritis[7, 8]. There were three issues in the xenograft model: (1) artificial stromal formation (low host reaction because of immunodeficiency, chimera status of mouse & human), (2) no early event of carcinogenesis and (3) rapid growth (leading to overestimation of the drug efficacy because clinical human cancer grows slowly). Therefore, we next used a mouse model of chemically induced skin cancer as a spontaneous tumor for the evaluation of anti-fibrin ADC[6] (Fig. 6A). Anti-fibrin ADC showed strong anti-tumor activity against this fibrin-rich tumor[6] (Fig. 6B and 6C). By in vivo fluorescence endomicroscopy, destroyed tumor vasculature was observed after the treatment[6] (Fig. 6D).

**Proof of concept study and future prospects**

We are now conducting two proof of concept (POC) studies: 1) The pathophysiological specificity of fibrin deposition in malignant diseases has been demonstrated in the immunohistological examination of various human tissues and animal disease models, and 2) the specificity of anti-fibrin mAb has also been validated in an immunoPET/CT imaging study by a third research group (Hisada *et al.*, unpublished data).

In this review, we have described the tumor stromal barrier and the development of CAST therapy. Besides the stromal barrier, microcirculation, inflammation or blood coagulation affects the pharmacokinetics and efficacy of antibody or ADC in the tumor microenvironment. Among these factors, microcirculation is very important because (1) it is the root between blood vessels and tumor cells (the stromal barrier limit microcirculation), and (2) it regulates tumor growth and metastasis (changes in the microcirculation context have direct effects on the efficacy of the drug). Therefore, we have to understand the mechanism of microcirculation-regulation by further investigation and identify methods of manipulation to develop innovative ADCs including CAST therapy.

## Acknowledgments and Funding

**Acknowledgements**

We thank Dr. T. Sugino, Y. Hisada, Dr. A. Tsuji and Dr. T. Saga for helpful discussions. We also thank Mrs. H. Koike and Mrs. M. Araake-MIzoguchi for technical assistance and Mrs. K. Shiina for secretarial support.

**Sources of Funding**

This work was supported by the Funding Program for World-Leading Innovative R&D on Science and Technology (FIRST Program) (YM), Third Term Comprehensive Control Research for Cancer from the Ministry of Health, Labour and Welfare of Japan (YM), Grant-in-Aid for Scientific Research on Priority Areas from the Ministry of Education, Culture, Sports, Science and Technology, the Princess Takamatsu Cancer Research Fund (YM), the Japanese Foundation for Multidisciplinary Treatment of Cancer (YM), the National Cancer Center Research and Development Fund (MY), the

Kobayashi Foundation Research Grant for Cancer Research (MY) and Grant-in-Aid for Scientific Research from the Japan Society for the Promotion of Science (MY).

**Disclosures**
None.

## References


1) Imai K, Takaoka A. Comparing antibody and small-molecule therapies for cancer. Nat Rev Cancer. 2006; **6**: 714-727.
2) Wu AM, Senter PD. Arming antibodies: prospects and challenges for immunoconjugates. Nat Biotechnol. 2005; **23**: 1137-1146.
3) Ricart AD, Tolcher AW. Technology insight: cytotoxic drug immunoconjugates for cancer therapy. Nat Clin Pract Oncol. 2007; **4**: 245-255.
4) Dirix LY, Rutten A, Huget P, Dirix M. Trastuzumab emtansine in breast cancer. Expert Opin Biol Ther. 2013; **13**: 607-614.
5) Matsumura Y. Cancer stromal targeting (CAST) therapy. Adv Drug Deliv Rev. 2012; **64**: 710-719.
6) Yasunaga M, Manabe S, Matsumura Y. New concept of cytotoxic immunoconjugate therapy targeting cancer-induced fibrin clots. Cancer Sci. 2011; **102**: 1396-1402.
7) Yasunaga M, Manabe S, Tarin D, Matsumura Y. Cancer stromal targeting therapy by cytotoxic immunoconjugate bound to the collagen IV network in the tumor tissue. Bioconjug Chem. 2011; **22**: 1776-1783.
8) Yasunaga M, Manabe S, Tarin D, Matsumura Y. Tailored immunoconjugate therapy depending on a quantity of tumor stroma. Cancer Sci. 2013; **104**: 231-237.
9) Grapin-Botton A, Melton DA. Endoderm development: from patterning to organogenesis. Trends Genet. 2000; **16**:124-130.
10) Rossi JM, Dunn NR, Hogan BL, Zaret KS. Distinct mesodermal signals, including BMPs from the septum transversum mesenchyme, are required in combination for hepatogenesis from the endoderm. Genes Dev. 2001; **15**: 1998-2009.
11) Yasunaga M, Nisikawa S. Production of endoderm-derived visceral organ cells from ES cells. Tanpakushitsu Kakusan Koso. 2007; **52**: 57-66.
12) Cheng CY, Mruk DD. The blood-testis barrier and its implications for male contraception. Pharmacol Rev. 2012; **64**: 16-64.
13) Dvorak HF, Senger DR, Dvorak AM. Fibrin as a component of the tumor stroma: origins and biological significance. Cancer Metastasis Rev. 1983; **2**: 41-73.
14) Liotta LA, Kohn EC. The microenvironment of the tumour-host interface. Nature. 2001; **411(6835)**: 375-379.
15) Marx J. Cancer biology. All in the stroma: cancer's Cosa Nostra. Science. 2008; **320**: 38-41.
16) Tarin D. Tissue interactions in morphogenesis, morphostasis and carcinogenesis J Theor Biol. 1972; **34**: 6172.
17) Tarin D, Price JE. Influence of microenvironment and vascular anatomy on "metastatic" colonization potential of mammary tumors. Cancer Res 1981; **41**: 36043609.
18) Matsumura Y, Maeda H. A new concept for macromolecular therapeutics in cancer chemotherapy: mechanism of tumoritropic accumulation of proteins and the antitumor agent smancs. Cancer Res. 1986; **46**: 6387-6392.
19) Nakahara T, Norberg SM, Shalinsky DR, Hu-Lowe DD, McDonald DM. Effect of inhibition of vascular endothelial growth factor signaling on distribution of extravasated antibodies in tumors. Cancer Res. 2006; **66**:1434-1445.
20) Lee CM, Tannock IF. The distribution of the therapeutic monoclonal antibodies cetuximab and trastuzumab within solid tumors. BMC Cancer. 2010 **10**:255.
21) Richmond A, Su Y. Mouse xenograft models vs GEM models for human cancer therapeutics. Dis Model Mech. 2008; **2-3**:78-82.
22) Olive KP, Jacobetz MA, Davidson CJ, Gopinathan A, McIntyre D, Honess D, *et al.* Inhibition of Hedgehog signaling enhances delivery of chemotherapy in a mouse model of pancreatic cancer. Science. 2009; **324**:1457-1461.
23) Dimou A, Syrigos KN, Saif MW. Overcoming the stromal barrier: technologies to optimize drug delivery in pancreatic cancer. Ther Adv Med Oncol. 2012; **5**:271-279.

IJC
International Journal of Cancer

# Effect of combined treatment with the epirubicin-incorporating micelles (NC-6300) and 1,2-diaminocyclohexane platinum (II)-incorporating micelles (NC-4016) on a human gastric cancer model

Yoshiyuki Yamamoto[1,2], Ichinosuke Hyodo[2], Misato Takigahira[1], Yoshikatsu Koga[1], Masahiro Yasunaga[1], Mitsunori Harada[3], Tatsuyuki Hayashi[3], Yasuki Kato[3] and Yasuhiro Matsumura[1]

[1] Division of Developmental Therapeutics, Research Center for Innovative Oncology, National Cancer Center Hospital East, Kashiwa, Chiba, Japan
[2] Department of Gastroenterology and Hepatology, Institute of Clinical Medicine, Graduate School of Comprehensive Human Sciences, University of Tsukuba, Tsukuba, Ibaraki, Japan
[3] Research Division, NanoCarrier Co., Ltd, Kashiwa, Chiba, Japan

**Anticancer agent-incorporating polymeric micelles accumulate effectively in tumors *via* the enhanced permeability and retention effect to exert potent antitumor effects. However, combined use of such micelles has not been elucidated. We compared the effect of combining the epirubicin-incorporating micelle NC-6300 and 1,2-diaminocyclohexane platinum (II) (oxaliplatin parent complex)-incorporating micelle NC-4016 (NCs) with that of epirubicin and oxaliplatin (E/O) in 44As3Luc cells using the combination index method. The *in vivo* antitumor activities of NCs and E/O were evaluated in mice bearing 44As3Luc xenografts. Pharmacokinetic analysis was performed by high-performance liquid chromatography and mass spectrometry. Cardiotoxicity of NC-6300 and epirubicin was assessed by echocardiography. Neurotoxicity of NC-4016 and oxaliplatin was evaluated by examining the paw withdrawal response to noxious mechanical stimuli. NCs showed a highly synergistic activity equivalent to E/O. *In vivo*, NCs exhibited higher antitumor activity in the subcutaneous tumor model and longer overall survival in the orthotopic tumor model than E/O ($p < 0.001$, $p = 0.015$, respectively). The intratumor concentrations of epirubicin and platinum were significantly higher following NCs than following E/O administration. Moreover, the micelles showed lower cardiotoxicity and neurotoxicity than the corresponding conventional drugs. The combined use of the micelles was associated with remarkable efficacy and favorable toxicities in the human gastric cancer model, and warrants the conduct of clinical trials.**



The therapeutic window of cytotoxic anticancer agents (ACAs) is known to be narrow; at concentrations falling outside this window, these agents either fail to work or cause severe adverse events. To overcome this drawback, drug delivery systems have been developed. By utilizing the enhanced permeability and retention (EPR) effect, based on the leaky blood vessels and impaired lymphatic drainage in tumor tissues, drug delivery systems in nanoparticle-form enable ACAs to accumulate selectively in the tumors and exert prominent antitumor effect while decreasing the toxicity of the drug payload.[1] Several preclinical studies have demonstrated the advantages of using ACA-incorporating polymeric micelles, and some are currently under clinical evaluation as single micelle agents alone[2–6] or single micelle agents in

**Key words:** gastric cancer, combination chemotherapy, polymeric micelle, NC-6300, NC-4016

**Abbreviations:** ACA: anticancer agent; ALT: alanine aminotransferase; AST, aspartate aminotransferase; BUN: blood urea nitrogen; CI: combination index; DACHP: 1,2-diaminocyclohexane platinum (II); DDS: drug delivery system; E/O: epirubicin and oxaliplatin; EF: ejection fraction; EPI: epirubicin; EPR effect: enhanced permeability and retention effect; Fa: the fractional-affected; HPLC: high-performance liquid chromatography; IC50: The 50% inhibitory concentration; ICP-MS: inductively coupled plasma mass spectrometry; NCs: NC-6300 and NC-4016; Pt: platinum; TV: the tumor volume

**Grant sponsors:** World-Leading Innovative R&D on Science and Technology, National Cancer Center Research and Development Fund, Ministry of Health, Labour and Welfare, Third Term Comprehensive Control Research for Cancer
**DOI:** 10.1002/ijc.28651
**History:** Received 16 Aug 2013; Accepted 15 Nov 2013; Online 3 Dec 2013

**Correspondence to:** Yasuhiro Matsumura, Division of Developmental Therapeutics, Research Center for Innovative Oncology, National Cancer Center Hospital East, 6-5-1 Kashiwanoha, Kashiwa, Chiba 277-8577, Japan, Tel.: +81-(0)-4-7133-1111 (Ex: 5400), Fax: +81-(0)-4-7134-6866, E-mail: yhmatsum@east.ncc.go.jp

**What's new?**
**Combination chemotherapy is sometimes associated with serious adverse effects that lead to treatment cessation. The combined use of anticancer agent-incorporating polymeric micelles–which enable anticancer agents to exert potent antitumor effects while decreasing the toxicity of the drug payload–may overcome this drawback. Reports of combined use of micellar anti-cancer agents are scarce, however. The present study showed that the combination of epirubicin- and DACHP-incorporating polymeric micelles had a stronger antitumor effect and lower toxicity in gastric cancer xenografts than combined epirubicin and oxaliplatin. These results warrant the conduct of clinical trials of combination treatments with anticancer agent-incorporating micelles.**

combination with nonmicelle conventional ACAs.[7–9] However, there are scarcely any reports of combined use of micellar ACAs.[10]

Gastric cancer has a poor prognosis, and represents the second leading cause of cancer mortality worldwide.[11] Although the survival times of patients with advanced gastric cancer have improved with advances in chemotherapy, they remain unsatisfactory.[12–15] The chemotherapeutic regimen for gastric cancer usually comprises a combination of two or three ACAs. While the EOX regimen (epirubicin, oxaliplatin and capecitabine) is considered to be one of the standard treatments in Europe,[13] the median overall survival of patients treated with EOX remains unsatisfactory at 11.2 months. When considering the tolerability, it would be difficult to add more cytotoxic agents to improve the therapeutic power of the EOX regimen. With regard to the use of molecular-targeted agents like everolimus and lapatinib, and of biologics such as cetuximab, panitumumab and bevacizumab, no survival benefit of the addition of these agents except for trastuzumab to the standard chemotherapy has been demonstrated in clinical trials for advanced gastric cancer.[16] Under these circumstances, we thought that the idea of replacing two or more of the key cytotoxic agents with their corresponding ACA-incorporating polymeric micelles may be of benefit for cancer patients.

Epirubicin, an anthracycline antitumor drug, has been approved for the treatment of various human cancers.[17,18] However, the anthracyclines have significant dose-limiting cardiotoxicity. Although epirubicin exerts ~33% lower cardiotoxicity than doxorubicin, it remains a serious clinical issue.[19] There are currently no effective therapies to prevent or reduce this cardiotoxicity. Against this background, NC-6300, polymeric micelles incorporating epibubicin was synthesized. NC-6300 comprises epirubicin covalently bound to polyethyleneglycol–poly(aspartiate) block copolymer through an acid–labile hydrazone bond. The conjugate spontaneously forms a micellar structure with a mean diameter of 60–70 nm in aqueous media.[20] *In vitro* findings indicated that it showed pH-dependent epirubicin release, namely, the release of epirubicin from NC-6300 accelerated under increasingly acidic conditions. Therefore the effective release of EPI may be expected within lysosomes of the cancer cells after intracellular trafficking. We have reported from preclinical studies that NC-6300 can reduce the cardiotoxicity of epirubicin and enhance its antitumor activity.[20,21] Oxaliplatin is a third-generation platinum drug that is associated with reduced renal toxicity and ototoxicity, which are typical adverse effects of the former-generation platinum drugs. On the other hand, it can cause troublesome peripheral neurotoxicities such as neuropathic pain and cold sensitivity; it has been reported that this neurotoxicity increases in severity as the cumulative dose of oxaliplatin increases, sometimes necessitating discontinuation of therapy in patients in whom the treatment has otherwise been effective.[22] To overcome this significant drawback of the drug, NC-4016, polymeric micelles incorporating 1,2-diaminocyclohexane platinum (II) (DACHP, the oxaliplatin parent complex) were synthesized. NC-4016 were spontaneously formed from the interaction of the platinum of DACHP and the carboxylic moieties of polyethyleneglycol–poly(glutamate) block copolymer. The mean particle size of NC-4016 is 30–40 nm in diameter. In media containing chloride ions, DACHP is released from the micelles through ligand exchange between the carboxylic groups in poly(glutamate) and the chloride ions. Previous studies have demonstrated the efficacy of NC-4016 against various cancer cell lines.[23,24]

In the present study, we evaluated the efficacy of the combined use of NC-6300 and NC-4016 (NCs) in comparison with that of the combined use of epirubicin and oxaliplatin (E/O) in mice bearing human gastric cancer xenografts.

## Material and Methods

### Drugs

NC-6300 and NC-4016 were prepared by NanoCarrier Co. (Kashiwa, Japan). Epirubicin was purchased from Pfizer Japan (Tokyo, Japan). Oxaliplatin was purchased from Yakult Honsha Co. (Tokyo, Japan).

### Cell cultures

44As3 is a human signet-ring cell gastric cancer cell line that spontaneously metastasizes to the peritoneal cavity and produces large volumes of bloody ascites after orthotopic implantation into the gastric wall.[25,26] A 44As3 cell line stably expressing firefly luciferase (44As3Luc) was established to evaluate tumor progression by *in vivo* imaging.[26] 44As3Luc was kindly provided by Dr. K. Yanagihara (National Cancer

Center Hospital East, Kashiwa, Japan). 44As3Luc cells were maintained in RPMI 1640 medium containing 10% fetal bovine serum (Cell Culture Technologies, Gaggenau-Hoerden, Germany), 100 units/mL penicillin, 100 μg/mL streptomycin and 25 μg/mL amphotericin B (Sigma, St. Louis, MO) in a humidified 5% $CO_2$ atmosphere at 37°C.

### *In vitro* growth-inhibition assay

The growth-inhibitory effects of NC-6300, NC-4016, epirubicin and oxaliplatin were examined by the tetrazolium salt-based proliferation assay (WST-8 assay; Wako Chemicals, Osaka, Japan). 44As3Luc cells were placed in 96-well plates at 3,000 cells/well in a final volume of 100 μL and incubated for 24 h at 37°C. The medium was then removed, and each drug was added in graded concentrations to the wells and incubated for 72 h at 37°C. After medium removal, WST-8 solution (10 μL) and medium (90 μL) were added to the wells, and the plates were incubated for 1 h at 37°C. The growth-inhibitory effects of each drug were assessed in a 96-well spectrophotometric plate reader (SpectraMax 190, Molecular Devices Corp., CA). The 50% inhibitory concentration ($IC_{50}$) was determined from the dose–response curves.

### Drug interaction analysis

The nature of the interactions between NCs, and between E/O against the 44As3Luc cells was evaluated by the combination index (CI) method of Chou and Talalay.[27] Data were analyzed using the Calcusyn software (Biosoft, NY). NC-6300 and NC-4016 or epirubicin and oxaliplatin were combined at fixed ratios spanning the individual $IC_{50}$ values of each of the agents. The $IC_{50}$ values were determined on the basis of the dose–response curves using the WST assay. For any given drug combination, the CI is known to represent the degrees of synergy, additivity and antagonism. It is expressed in terms of the fractional-affected (*Fa*) value, which represents the percentage of cells killed or inhibited by the drug. *Fa*/CI plots were constructed by computer analysis of the data generated from the median effect analysis.

### *In vivo* subcutaneous models

Female BALB/c nu/nu mice were purchased from Japan SLC (Shizuoka, Japan). They were maintained under specific-pathogen-free conditions under a 12/12-h light/dark cycle and provided free access to sterile food, water and cages. Eight-week-old mice were subcutaneously inoculated with $5 \times 10^5$ 44As3Luc cells in the flank region. On the day the tumor volume reached 300 $mm^3$, the mice were randomly divided into seven test groups consisting of five mice each (Day 0). The test drugs were administered intravenously on Days 0, 7 and 14 *via* the lateral tail vein. The single-agent therapy groups received NC-6300 8 mg/kg (on an epirubicin basis) or epirubicin 8 mg/kg, or NC-4016 4 mg/kg (on an oxaliplatin basis) or oxaliplatin 4 mg/kg. The combined therapy groups received a combination of NC-6300 8 mg/kg plus NC-4016 4 mg/kg, or epirubicin 8 mg/kg plus oxaliplatin 4 mg/kg. The normal control group received 5% dextrose solution. The length (*a*) and width (*b*) of the tumor masses were measured twice each week, and the tumor volume (TV) was calculated using the following equation: $TV = (a \times b^2)/2$. For humane reasons, the animals in which the tumor volume exceeded 2,000 $mm^3$ were sacrificed. All animal procedures were performed in compliance with the Guidelines for the Care and Use of Experimental Animals established by the Committee for Animal Experimentation of the National Cancer Center; these guidelines meet the ethical standards required by law and also comply with the guidelines for the use of experimental animals in Japan.

### *In vivo* orthotopic models

A total of $1 \times 10^6$ 44As3Luc cells were inoculated into the gastric wall of each 6-week-old female BALB/c nu/nu mouse after laparotomy, as described previously.[25,26,28] Seven days after the inoculation (Day 0), the mice were randomly divided into three groups of eight mice each. Randomization was performed on the basis of the bioluminescence images, and the mean values of count per minute were confirmed to be statically identical among the groups. The drugs of each combination therapy were administered at the same doses/*via* the same route as in the aforementioned study using the subcutaneous tumor models, on Days 0, 7 and 14. Control mice were injected with 5% dextrose solution on the same schedule. *In vivo* photon counting analysis was conducted on a cryogenically cooled IVIS system using the Living Image software (Caliper Life Sciences, MA). *In vivo* bioluminescence imaging was performed twice each week from the day of treatment initiation. The body weight of each mouse was also measured. Mortality was checked daily.

### Pharmacokinetic analysis

Eighteen days after the inoculation of the 44As3Luc cells into the gastric wall, a pharmacokinetic study was conducted in the female BALB/c nu/nu nude mice. The animals were injected with a combination of NC-6300 8 mg/kg plus NC-4016 4 mg/kg or epirubicin 8 mg/kg plus oxaliplatin 4 mg/kg intravenously. Under general anesthesia, blood was collected *via* cardiac puncture, and the gastric tumor, liver, spleen, kidneys, heart and small intestine were excised at 0.17, 1, 6, 24, 48, 72 and 168 h, respectively, after the drug administration. Pharmacokinetic analysis was conducted using three mice for each time point.

The epirubicin concentrations derived from NC-6300 and conventional epirubicin in each tissue were measured by high-performance liquid chromatography (HPLC) (RF-20AXS, Shimadzu Corporation, Kyoto, Japan). For the case of NC-6300, the concentrations of both the free epirubicin (*i.e.*, that released *in vivo* from NC-6300) and total epirubicin (*i.e.*, that released from NC-6300 plus the remainder of NC-6300) were determined as described previously.[20]

The platinum concentrations derived from NC-4016 and oxaliplatin in each tissue were determined using inductively

coupled plasma mass spectrometry (ICP-MS) (SPG9000, Seiko Instruments, Tokyo, Japan). Platinum concentration in each tissues was measured at 0.17, 6 and 24 h after the intravenous injection. For the quantitative determination of platinum content, blood samples were centrifuged at 1600 G for 15 min, and then plasma was diluted with 0.1% $HNO_3$. The other tissue samples were digested with a mixture of 98% $H_2SO_4$ and 62% $HNO_3$ (1:2, v:v) and then analyzed by ICP.

### Hematotoxicity, hepatotoxicity and nephrotoxicity of the combination therapies

Eight-week-old female CD1 (ICR) mice (Charles River Japan, Kanagawa, Japan) were randomly divided into two groups (Day 0). The drugs of each combination therapy were administered at the same doses/*via* the same route as for the *in vivo* tumor growth inhibition assay, on Days 0, 7 and 14. Blood samples were taken every 7 days from three mice in each group *via* cardiac puncture under general anesthesia. In each blood sample, the white blood cells (WBCs), red blood cells (RBCs) and platelets were counted using Celltac α MEK-6358 (NIHON KODEN, Tokyo, Japan). In addition, the plasma concentrations of aspartate aminotransferase (AST), alanine aminotransferase (ALT), blood urea nitrogen (BUN) and creatinine were measured in SRL Laboratories (Tokyo, Japan).

### Cardiotoxicity of NC-6300 versus epirubicin

To compare the cardiotoxicities of NC-6300 and epirubicin, 7-week-old female C57BL/6NCr mice ($n = 7$; Japan SLC, Shizuoka, Japan) were administered NC-6300 8 mg/kg or epirubicin 8 mg/kg on Days 0, 7 and 14 every 4 weeks over a period of 8 weeks (six doses in total). Control mice were injected with 5% dextrose solution on the same schedule. Echocardiography was performed once per week using a high-resolution Micro Ultrasound system (Vevo 770, VisualSonics, Toronto, Canada) equipped with a 40-MHz ultrasound probe (RMV704, VisualSonics). The mice were kept under light sedation with 1–2% isoflurane until the heart rate stabilized from 350 to 450 beats per minute. The left-ventricular dimensions and wall thickness were measured on the parasternal long-axis views, and the ejection fraction (EF) was automatically calculated from the structural parameters using the Vevo 770 software.

### Neurotoxicity of NC-4016 versus oxaliplatin

We investigated the neurotoxicities of NC-4016 and oxaliplatin using the nocifensive behavior of paw withdrawal from noxious mechanical stimuli.[29] Six-week-old female DBA/2N mice (Charles River Japan, Kanagawa, Japan) were randomly divided into three groups, and their baseline nocifensive responses were measured. The mean latency was confirmed to be statically identical among the groups. The mice ($n = 9$) were then administered NC-4016 4 mg/kg or oxaliplatin 4 mg/kg on Days 0, 7 and 14 every 4 weeks over a period of 12 weeks (nine doses in total). Control mice were injected with 5% dextrose solution on the same schedule. After the nine administrations in total, the nocifensive responses in each group were measured again. Mechanical allodynia was assessed by measuring the latency of the paw withdrawal in response to noxious mechanical stimuli using a dynamic plantar esthesiometer (Ugo Basile, Varese, Italy). The mice were placed on a wire mesh floor in individual Plexiglas cages and allowed to acclimate for ~1 h, during which exploratory and grooming activity ended. A mechanical stimulus was applied to the plantar aspect of the hind paw using a metal filament with 2-mm diameter. The force was automatically increased at a fixed rate (0–5 g, 0.25 g/s) until the mouse withdrew its paw. The elicitations of the paw withdrawal responses were repeated four times at 10-s intervals. The paw withdrawal threshold (g) was calculated as the average of four measurements.

### Statistical analysis

Data are expressed as mean ± SD. Repeated-measures ANOVA was used to evaluate the antitumor effects of the drugs and the changes in the body weight and cardiac function of each treatment group. Survival was assessed using the Kaplan–Meier method. Student's *t*-test was used to compare the nadir values of the blood cell counts. ANOVA with Tukey's multiple comparison was used to evaluate the changes in the nocifensive responses. The level of significance for all tests was set at $p < 0.05$. All statistical tests were two-sided. All analyses were conducted using SPSS, version 19.0 (SPSS, Chicago, IL).

## Results

### *In vitro* growth-inhibition assay

The $IC_{50}$ values of NC-6300 and NC-4016 for the 44As3Luc cells were 55 ± 2.3 nM and 374 ± 19 nM, respectively. The $IC_{50}$ values of epirubicin and oxaliplatin for the 44As3Luc cells were 15 ± 1.3 nM and 169 ± 13 nM, respectively. On the basis of these data, a molar ratio 1:10 was used for the NC-6300:NC-4016 and epirubicin:oxaliplatin combination studies.

### Drug interactions between NC-6300 and NC-4016 (NCs) and between epirubicin and oxaliplatin (E/O)

Combination indices (CIs) of <1.0, 1.0 and >1.0 are indicative of synergistic, additive and antagonistic interactions between two agents, respectively. Marked synergism with a CI of 0.98–0.35 was observed between *Fa* 0.5 and 1.0 in both combination groups. The synergistic effect of NCs (Fig. 1*a*) was almost equivalent to that of E/O (Fig. 1*b*).

### *In vivo* antitumor effect of single agents and combinations

*Subcutaneous tumor.*

The therapeutic effect of NC-6300 was significantly greater than that of epirubicin ($p = 0.047$). Similarly, the effect of NC-4016 was significantly greater than that of oxaliplatin ($p = 0.023$). The therapeutic effect of E/O was significantly

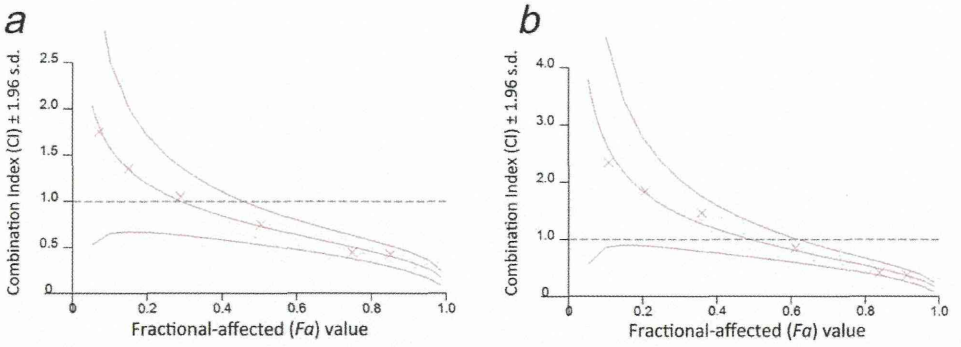


| NC-6300 + NC-4016 | | | |
|---|---|---|---|
| *Fa* | 0.5 | 0.75 | 0.9 |
| CI | 0.732 | 0.503 | 0.349 |

| Epirubicin + Oxaliplatin | | | |
|---|---|---|---|
| *Fa* | 0.5 | 0.75 | 0.9 |
| CI | 0.981 | 0.613 | 0.391 |

**Figure 1.** CIs of the combined micelle (*a*) and free ACA regimens (*b*). CIs of <1.0, 1.0 and ≥1.0 are indicative of synergistic interactions, additive interactions and antagonism, respectively. NCs exhibited synergistic activity equivalent to E/O between *Fa* 0.5 and 1.0.

greater than that of epirubicin alone ($p = 0.001$) and oxaliplatin alone ($p = 0.002$). Likewise, the therapeutic effect of NCs was significantly greater than that of NC-6300 alone ($p < 0.001$) and NC-4016 alone ($p < 0.001$). Furthermore, the therapeutic effect of NCs was significantly greater than that of E/O ($p < 0.001$) (Fig. 2*a*).

There were slight and transient, but significant differences in the body weight loss between the single-agent and combined treatment groups (date not shown).

*Orthotopic tumor*

Comparison of the relative photon count until Day 28 in the 44As3Luc orthotopic model revealed that the antitumor effect of NCs was greater than that of E/O ($p = 0.016$). The antitumor effect of E/O was greater than that of control ($p < 0.001$) (Figs. 2*b* and 2*c*). On Day 28 after the initiation of each treatment, the localizations of the tumor in mice treated with NCs were restricted to the stomach of the primary site. On the other hand, widespread disseminations in the abdominal cavity were observed in the other two groups (Fig. 2*c*). The survival rate in the NCs group was also significantly superior to that in the E/O group ($p = 0.015$). Whereas there was no significant improvement between the E/O and control groups ($p = 0.173$) (Fig. 2*d*). There was no difference in the body weight loss or toxic death date between the two combined treatment groups (Fig. 2*e*).

### Pharmacokinetic analysis

Next, we examined the concentration–time profiles of epirubicin and platinum in the plasma and various tissues of the mice after NCs and E/O administration. After E/O administration, the concentration of native epirubicin in the plasma and tumor decreased rapidly and the drug disappeared from both within 48 h. The $C_{max}$ in the tumor was reached at 1 h after the injection. In contrast, after NCs administration, the highest intratumor concentration of free epirubicin released from NC-6300 was observed at 24 h, with the drug concentration remaining high for 3 days (Fig. 3*a*). NC-6300 was stable in the plasma and the amount of epirubicin released into the plasma was small (5%). The areas under the curve (AUC) ratios of free epirubicin released from NC-6300 to native epirubicin were 2.11, 3.78 and 4.99 in the tumor, plasma and liver, respectively. In contrast, the corresponding AUC ratio was only 0.27 in the heart. Furthermore, 42–53% epirubicin was released from NC-6300 in the normal tissues examined, while 81% was released in the tumor. The AUC of the epirubicin released in the liver was about fivefold greater than that of native epirubicin (Table 1).

Platinum derived from oxaliplatin cleared rapidly from the plasma and tumor after E/O administration (Fig. 3*b*). In contrast, platinum derived from NC-4016 after NCs administration gradually increased in the tumor and decreased in the plasma. The AUC ratios of platinum derived from NC-4016 to oxaliplatin were 3.69, 42.82 and 1.16 in the tumor, plasma and liver, respectively (Table 2). The platinum levels in the heart and small intestine were below the minimum limit of detection in both combination groups, and could not be evaluated.

### Hematotoxicity, hepatotoxicity and nephrotoxicity of the combination therapies

The nadirs of the WBC and RBC counts in the E/O group were significantly lower than those in the NCs group ($p = 0.027$ and 0.007, respectively) (Fig. 4*a*). Slight and transient elevation of the hepatic transaminases was observed after the administration of NCs (Fig. 4*b*). No nephrotoxicity was observed in either group (Fig. 4*b*).

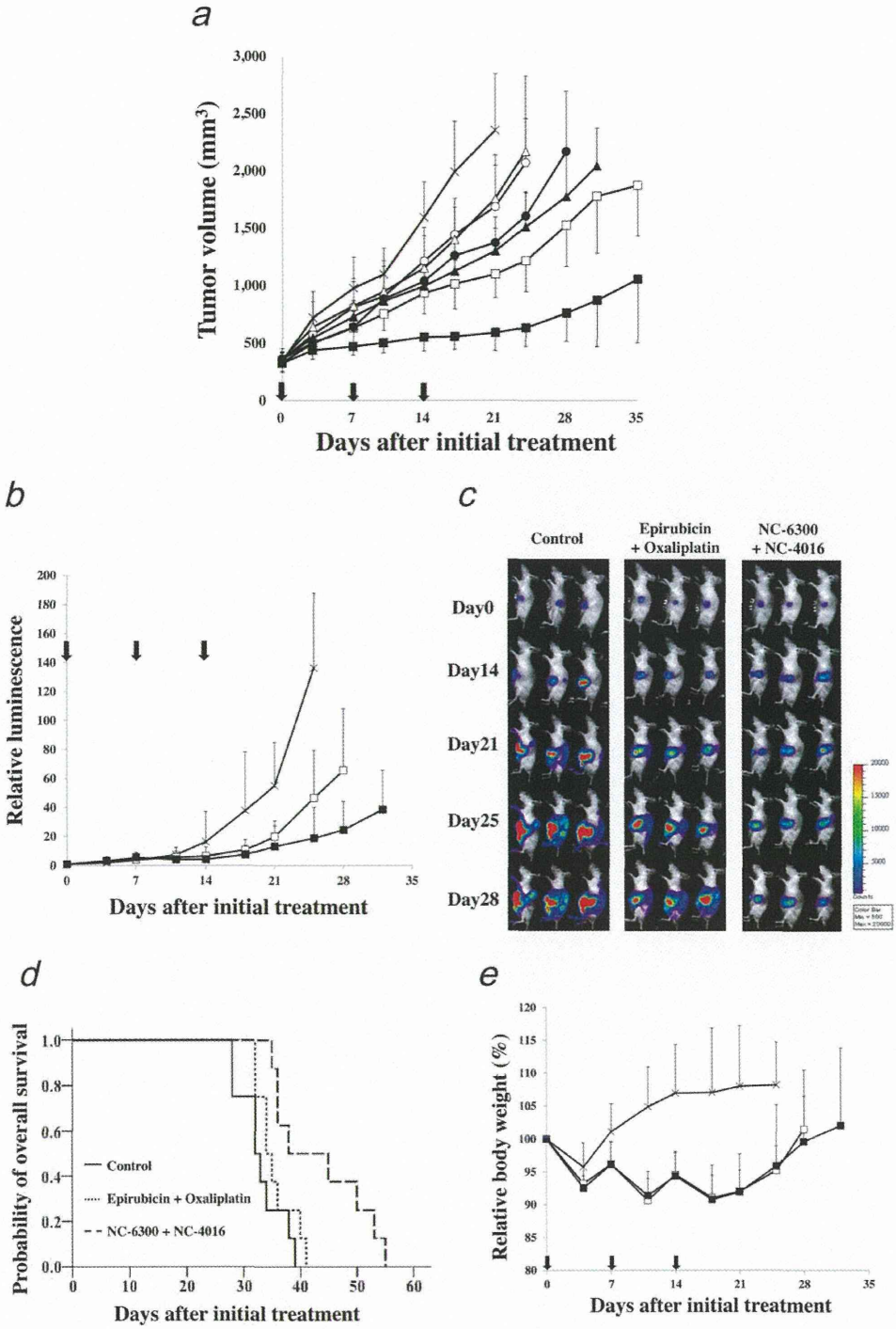


Figure 2. *In vivo* tumor growth inhibition assay. (*a*) Subcutaneous 44As3Luc xenograft models. The treatments were administered on Days 0, 7 and 14 after the tumor volume reached 300 $mm^3$ (Day 0) ($n = 5$). (×) Control, (○) epirubicin 8 mg/kg, (△) oxaliplatin 4 mg/kg, (□) epirubicin 8 mg/kg plus oxaliplatin 4 mg/kg, (●) NC-6300 8 mg/kg, (▲) NC-4016 4 mg/kg, (■) NC-6300 8 mg/kg plus NC-4016 4 mg/kg. *Points*, mean; *bars*, SD; *arrows*, drug injections. (*b–e*) Orthotopic 44As3Luc xenograft models. Seven days after the inoculation of 44As3Luc cells into the gastric wall (Day 0), the treatments were administered on Days 0, 7 and 14 ($n = 8$). (×) Control, (□) epirubicin 8 mg/kg plus oxaliplatin 4 mg/kg, (■) NC-6300 8 mg/kg plus NC-4016 4 mg/kg. (*b*,*c*) The antitumor activities using a photon-imaging system. *Points*, mean; *bars*, SD; *arrows*, drug injections. (*d*) Kaplan–Meier curves of mice bearing orthotopic 44As3Luc xenografts. (*e*) Changes in the relative body weight. *Points*, mean; *bars*, SD; *arrows*, drug injections.

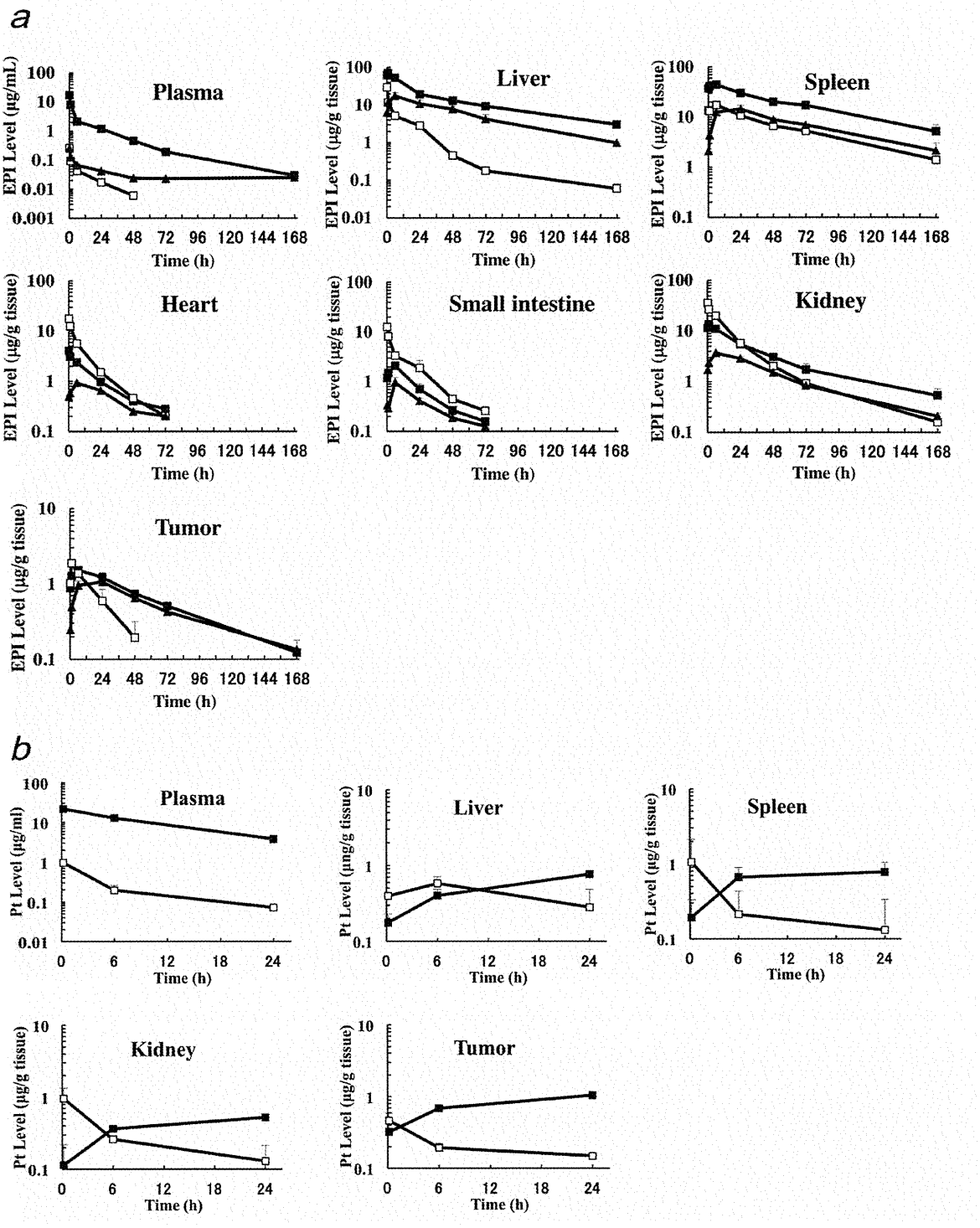


Figure 3. (*a*) Plasma and tissue concentration–time profiles of epirubicin (EPI) analyzed by HPLC after a single administration of NCs or E/O to mice bearing orthotopic 44As3Luc xenografts ($n = 3$). (□) Native epirubicin level from epirubicin 8 mg/kg plus oxaliplatin 4 mg/kg, (▲) released epirubicin level from NC-6300 8 mg/kg plus NC-4016 4 mg/kg, (■) total epirubicin level from NC-6300 8 mg/kg plus NC-4016 4 mg/kg. *Points*, mean; *bars*, SD. (*b*) Plasma and tissue concentration–time profiles of platinum (Pt) analyzed by ICP-MS after a single administration of NCs or E/O to mice bearing orthotopic 44As3Luc xenografts ($n = 3$). (□) Platinum level from epirubicin 8 mg/kg plus oxaliplatin 4 mg/kg, (■) platinum level from NC-6300 8 mg/kg plus NC-4016 4 mg/kg. *Points*, mean; *bars*, SD.

Table 1. AUC values of epirubicin in plasma and tissues after injection of NCs or E/O in mice bearing orthotopic 44As3Luc xenografts

| | AUC (mg/g tissue or mL × h) | | | | |
|---|---|---|---|---|---|
| | NC-6300 | | | | |
| | Released epirubicin | Total epirubicin | % Released | Native epirubicin | Released/native epirubicin AUC ratio |
| Plasma | 5.3 | 104.9 | 5.0 | 1.4 | 3.78 |
| Liver | 954.7 | 2269.1 | 42.1 | 191.7 | 4.98 |
| Spleen | 1201.5 | 3048.0 | 39.4 | 1017.7 | 1.18 |
| Kidney | 206.7 | 491.8 | 42.0 | 559.7 | 0.37 |
| Heart | 44.2 | 84.8 | 52.1 | 164.8 | 0.27 |
| Small intestine | 32.7 | 61.5 | 53.2 | 134.2 | 0.24 |
| Tumor | 82.1 | 100.9 | 81.4 | 38.8 | 2.11 |

Table 2. AUC values of platinum in plasma and tissues after injection of NCs or E/O in mice bearing orthotopic 44As3Luc xenografts

| | AUC (mg/g tissue or mL × h) | | |
|---|---|---|---|
| | Platinum (Pt) from NC-4016 | Platinum (Pt) from oxaliplatin | Pt (NC-4016)/Pt (oxaliplatin) AUC ratio |
| Plasma | 253.03 | 5.91 | 42.82 |
| Liver | 12.30 | 10.64 | 1.16 |
| Spleen | 15.46 | 6.83 | 2.26 |
| Kidney | 9.39 | 7.08 | 1.33 |
| Tumor | 18.56 | 5.03 | 3.69 |

### Cardiotoxicity and neurotoxicity

We assessed the cardiotoxicity induced by NC-6300 and epirubicin by transthoracic echocardiography. The EF was maintained within normal range in the mice treated with NC-6300 during and after the six administrations, and there was no difference in the EF between the NC-6300 treatment group and control group ($p = 0.076$). Whereas the mice treated with epirubicin exhibited a significantly lower EF than the NC-6300 treatment group ($p < 0.001$) and control group ($p < 0.001$) (Fig. 4*c*).

We next analyzed mechanical allodynia. After a total of nine administrations of each drug, the mice in the oxaliplatin treatment group exhibited a significantly lower mechanical threshold than the mice in the control group ($p < 0.001$) and NC-4016 treatment group ($p = 0.002$) (Fig. 4*d*). There was no statistically significant difference in the mechanical thresholds between the NC-4016 treatment group and control group ($p = 0.820$).

## Discussion

Co-administration of anthracycline-based topoisomerase II inhibitors and platinum-based DNA-modifying agents is widely used in clinical practice.[13,30,31] The synergism between these two classes of drugs can be explained by the reciprocal interaction in which the inhibition of topoisomerase II partially hinders the efficient repair of DNA damaged by platinum alkylating agents.[32–34] In the present study, NCs exhibited synergistic activity equivalent to E/O. This suggests that the effective drug interaction between epirubicin and oxaliplatin was conserved *in vitro* in the combination of the corresponding micelles. Moreover, NCs exhibited significantly greater antitumor activity than E/O in the subcutaneous and orthotopic tumor models.

The pharmacokinetic analysis revealed that the AUCs of both epirubicin and platinum in the tumor tissue were greater following NCs administration than those following E/O administration, which clearly indicates that co-administration of two micellar formulations does not dampen their EPR effect in the tumors. NC-6300 and NC-4016 are very similar in terms of their mean micelle size, and the micellar surfaces are not modified with specific therapeutic components such as antibody, ligand or peptide. It remains unclear how the EPR effect might be influenced if micelles of differing sizes and/or surface-modified micelles were used in combination.

In regard to the toxicity evaluation, the degree of weight loss was almost the same between the NCs and E/O groups. Leukopenia and anemia were significantly milder in the NCs group than in the E/O group. Slight elevation of the hepatic transaminases was observed only in the NCs group. This hepatotoxicity has also been reported to be observed following administration of cisplatin-incorporating micelles.[35] Following systemic administration, micelles are likely to be distributed predominantly in the liver due to the developed mononuclear phagocytotic system of the liver and the rough filtration of relatively large molecules through the fenestrated sinusoidal endothelium. However, the hepatotoxicity is generally mild and transient, because most of the drug released from the micelles exists in the Kupffer cells rather than in the hepatocytes, as reported previously.[36] We also evaluated the cumulative toxicity induced by epirubicin and oxaliplatin. Patients treated successfully by long-term administration of these drugs sometimes need discontinuation of the effective drug due to its cumulative toxicity. Epirubicin and oxaliplatin have specific cumulative dose-limiting toxicities, namely, cardiotoxicity and peripheral neuropathy, respectively. Both toxicities were clearly and significantly lower in severity in the

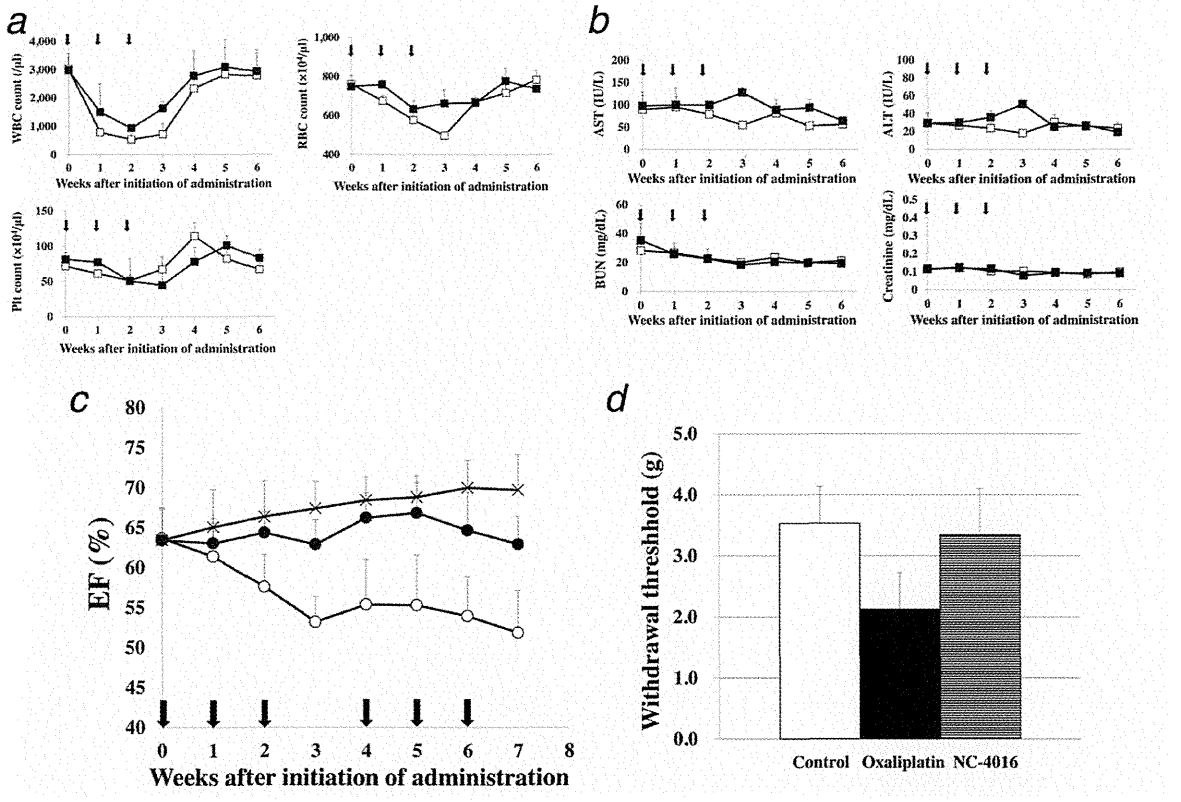


Figure 4. Toxicity assessment. (*a*) Hematotoxicity, (*b*) hepatotoxicity and nephrotoxicity. CD1 mice were given NCs or E/O on Days 0, 7 and 14. Blood samples were taken every 7 days from the day of treatment initiation ($n = 3$). (□) Epirubicin 8 mg/kg plus oxaliplatin 4 mg/kg, (■) NC-6300 8 mg/kg plus NC-4016 4 mg/kg. *Points*, mean; *bars*, SD; *arrows*, drug injections. (*c*) Cardiotoxicity evaluated using echocardiography. C57BL/6 mice ($n = 7$) were given NC-6300 or epirubicin on Days 0, 7 and 14 every 4 weeks over a period of 8 weeks (six administrations in total). (×) Control, (○) epirubicin 8 mg/kg, (●) NC-6300 8 mg/kg. *Points*, mean; *bars*, SD; *arrows*, drug injections. (*d*) Mechanical allodynia after a total of nine administrations. DBA/2N mice ($n = 9$) were given NC-4016 4 mg/kg or oxaliplatin 4 mg/kg on Days 0, 7 and 14 every 4 weeks over a period of 12 weeks. Mechanical allodynia was assessed by examining the paw withdrawal response to noxious mechanical stimuli using a dynamic plantar esthesiometer. *Bars*, SD.

micelle treatment group than in the conventional ACA treatment group. These findings were consistent with the findings of our previous study.[21,35] From these results, the combined micelle therapy could be expected to prolong the effective treatment duration, consequently leading to survival prolongation.

Multidrug regimens have been developed to enhance the anticancer efficacy and suppress the emergence of drug resistance. However, patients receiving such multidrug regimens sometimes experience additional and stronger drug adverse effects that could necessitate discontinuation of the treatment. In this regard, combined use of ACA-incorporating polymeric micelles may be a good alternative therapeutic modality, because micellar formulations are delivered selectively to tumor tissues *via* the EPR effect while their distribution to normal tissues is suppressed. Several types of nanoparticles, in which multiple ACAs are loaded on to one particle, have been developed recently and been shown to exhibit potent anticancer activity.[33,34,37,38] These fixed drug-ratio combinations are designed to maintain synergistic molar ratios to enhance the therapeutic benefit, and these multidrug-loaded nanoparticles may be useful in future clinical applications. However, there are some clinical concerns that need to be addressed in regard to this type of nanoparticles. Since the drugs are loaded in a fixed ratio prior to administration, flexible adjustment of the doses of each component drug encapsulated in the particles according to the profiles and severity of the emerging toxicities is difficult. Moreover, the types of cancer that are suitable for such treatments are likely limited. On the other hand, in the case of combined use of single drug-loaded micelles, it is easier to adjust the dose ratio and modify the dose of each micellar preparation as necessary during treatment.

Various ACA-incorporating micelles have been developed, and some are under investigation in clinical trials.[4–6] A phase III trial of NK105, a paclitaxel-incorporating micelle, is now underway for patients with metastatic breast cancer. In conclusion, it was demonstrated in the present preclinical study

that NCs exerted a stronger antitumor effect and lower toxicity in a human gastric cancer model as compared to E/O. Therefore, these results warrant further clinical evaluation of combination treatment with ACA-incorporating micelles.

## Acknowledgements

This work was supported by the Funding Program for World-Leading Innovative R&D on Science and Technology (FIRST Program) (to Y.M.), National Cancer Center Research and Development Fund (to Y.M.), and Ministry of Health, Labour and Welfare, Health and Labour Science Research Grants, Third Term Comprehensive Control Research for Cancer (to Y.M.). Y.Y. thanks the Foundation for Promotion of Cancer Research (Japan) for the Third-Term Comprehensive Control Research for Cancer for awarding him a research resident fellowship. We thank Dr. M. Yokoyama and Dr. K. Shiraishi (The Jikei University School of Medicine, Tokyo, Japan) for their support regarding PK study. We also thank Mrs. K. Shiina for her secretarial assistance.

## References

1. Matsumura Y, Maeda H. A new concept for macromolecular therapeutics in cancer chemotherapy: mechanism of tumoritropic accumulation of proteins and the antitumor agent smancs. *Cancer Res* 1986;46:6387–92.
2. Matsumura Y, Kataoka K. Preclinical and clinical studies of anticancer agent-incorporating polymer micelles. *Cancer Sci* 2009;100:572–9.
3. Matsumura Y. Preclinical and clinical studies of NK012, an SN-38-incorporating polymeric micelles, which is designed based on EPR effect. *Adv Drug Deliv Rev* 2011;63:184–92.
4. Plummer R, Wilson RH, Calvert H, et al. A Phase I clinical study of cisplatin-incorporated polymeric micelles (NC-6004) in patients with solid tumours. *Br J Cancer* 2011;104:593–8.
5. Kato K, Chin K, Yoshikawa T, et al. Phase II study of NK105, a paclitaxel-incorporating micellar nanoparticle, for previously treated advanced or recurrent gastric cancer. *Invest New Drugs* 2012;30:1621–7.
6. Hamaguchi T, Doi T, Eguchi-Nakajima T, et al. Phase I study of NK012, a novel SN-38-incorporating micellar nanoparticle, in adult patients with solid tumors. *Clin Cancer Res* 2010; 16:5058–66.
7. Nakajima TE, Yasunaga M, Kano Y, et al. Synergistic antitumor activity of the novel SN-38-incorporating polymeric micelles, NK012, combined with 5-fluorouracil in a mouse model of colorectal cancer, as compared with that of irinotecan plus 5-fluorouracil. *Int J Cancer* 2008;122: 2148–53.
8. Nagano T, Yasunaga M, Goto K, et al. Antitumor activity of NK012 combined with cisplatin against small cell lung cancer and intestinal mucosal changes in tumor-bearing mouse after treatment. *Clin Cancer Res* 2009;15:4348–55.
9. Nagano T, Yasunaga M, Goto K, et al. Synergistic antitumor activity of the SN-38-incorporating polymeric micelles NK012 with S-1 in a mouse model of non-small cell lung cancer. *Int J Cancer* 2010;127:2699–706.
10. Na HS, Lim YK, Jeong YI, et al. Combination antitumor effects of micelle-loaded anticancer drugs in a CT-26 murine colorectal carcinoma model. *Int J Pharm* 2010;383:192–200.
11. Ferlay J, Shin HR, Bray F, et al. Estimates of worldwide burden of cancer in 2008: GLOBOCAN 2008. *Int J Cancer* 2010;127:2893–917.
12. van Cutsem E, Moiseyenko VM, Tjulandin S, et al. Phase III study of docetaxel and cisplatin plus fluorouracil compared with cisplatin and fluorouracil as first-line therapy for advanced gastric cancer: a report of the V325 study group. *J Clin Oncol* 2006;24:4991–7.
13. Cunningham D, Starling N, Rao S, et al. Capecitabine and oxaliplatin for advanced esophagogastric cancer. *N Engl J Med* 2008;358:36–46.
14. Koizumi W, Narahara H, Hara T, et al. S-1 plus cisplatin versus S-1 alone for first-line treatment of advanced gastric cancer (SPIRITS trial): a phase III trial. *Lancet Oncol* 2008;9:215–21.
15. Bang YJ, van Cutsem E, Feyereislova A, et al. Trastuzumab in combination with chemotherapy versus chemotherapy alone for treatment of HER2-positive advanced gastric or gastro-oesophageal junction cancer (ToGA): a phase 3, open-label, randomised controlled trial. *Lancet* 2010;376:687–97.
16. Waddell T, Chau I, Cunningham D, et al. Epirubicin, oxaliplatin, and capecitabine with or without panitumumab for patients with previously untreated advanced oesophagogastric cancer (REAL3): a randomised, open-label phase 3 trial. *Lancet Oncol* 2013;14:481–9.
17. Llovet JM, Bruix J. Systematic review of randomized trials for unresectable hepatocellular carcinoma: chemoembolization improves survival. *Hepatology* 2003;37:429–42.
18. Roche H, Fumoleau P, Spielmann M, et al. Sequential adjuvant epirubicin-based and docetaxel chemotherapy for node-positive breast cancer patients: the FNCLCC PACS 01 Trial. *J Clin Oncol* 2006;24:5664–71.
19. de Azambuja E, Paesmans M, Beauduin M, et al. Long-term benefit of high-dose epirubicin in adjuvant chemotherapy for node-positive breast cancer: 15-year efficacy results of the Belgian multicentre study. *J Clin Oncol* 2009;27:720–5.
20. Harada M, Bobe I, Saito H, et al. Improved antitumor activity of stabilized anthracycline polymeric micelle formulation, NC-6300. *Cancer Sci* 2011;102:192–9.
21. Takahashi A, Yamamoto Y, Yasunaga M, et al. NC-6300, an epirubicin-incorporating micelle, extends the antitumor effect and reduces the cardiotoxicity of epirubicin. *Cancer Sci* 2013;104: 920–5.
22. de Gramont A, Figer A, Seymour M, et al. Leucovorin and fluorouracil with or without oxaliplatin as first-line treatment in advanced colorectal cancer. *J Clin Oncol* 2000;18:2938–47.
23. Cabral H, Nishiyama N, Okazaki S, et al. Preparation and biological properties of dichloro(1,2-diaminocyclohexane)platinum(II) (DACHPt)-loaded polymeric micelles. *J Controlled Release* 2005;101:223–32.
24. Cabral H, Nishiyama N, Kataoka K. Optimization of (1,2-diamino-cyclohexane)platinum(II)-loaded polymeric micelles directed to improved tumor targeting and enhanced antitumor activity. *J Controlled Release* 2007;121:146–55.
25. Yanagihara K, Takigahira M, Tanaka H, et al. Development and biological analysis of peritoneal metastasis mouse models for human scirrhous stomach cancer. *Cancer Sci* 2005;96: 323–32.
26. Yanagihara K, Takigahira M, Takeshita F, et al. A photon counting technique for quantitatively evaluating progression of peritoneal tumor dissemination. *Cancer Res* 2006;66:7532–9.
27. Chou TC, Talalay P. Quantitative analysis of dose-effect relationships: the combined effects of multiple drugs or enzyme inhibitors. *Adv Enzyme Regul* 1984;22:27–55.
28. Nakajima TE, Yanagihara K, Takigahira M, et al. Antitumor effect of SN-38-releasing polymeric micelles, NK012, on spontaneous peritoneal metastases from orthotopic gastric cancer in mice compared with irinotecan. *Cancer Res* 2008;68: 9318–22.
29. Renn CL, Carozzi VA, Rhee P, et al. Multimodal assessment of painful peripheral neuropathy induced by chronic oxaliplatin-based chemotherapy in mice. *Molecular Pain* 2011;7:29.
30. Martoni A, Bellucco A, Canova N, et al. Four-year analysis of platinum and anthracycline combination for ovarian cancer. *Oncology* 1989;46: 109–16.
31. Thigpen JT, Brady MF, Homesley HD, et al. Phase III trial of doxorubicin with or without cisplatin in advanced endometrial carcinoma: a gynecologic oncology group study. *J Clin Oncol* 2004;22:3902–8.
32. Scambia G, de Vincenzo R, Ranelletti FO, et al. Antiproliferative effect of silybin on gynaecological malignancies: synergism with cisplatin and doxorubicin. *Eur J Cancer* 1996;32A:877–82.
33. Lee SM, O'Halloran TV, Nguyen ST. Polymer-caged nanobins for synergistic cisplatin-doxorubicin combination chemotherapy. *J Am Chem Soc*, 2010;132:17130–8.
34. Xiao H, Li W, Qi R, et al. Co-delivery of daunomycin and oxaliplatin by biodegradable polymers for safer and more efficacious combination therapy. *J Controlled Release*, 2012; 163:304–14.
35. Uchino H, Matsumura Y, Negishi T, et al. Cisplatin-incorporating polymeric micelles (NC-6004) can reduce nephrotoxicity and neurotoxicity of cisplatin in rats. *Br J Cancer* 2005;93:678–87.
36. Takahashi A, Ohkohchi N, Yasunaga M, et al. Detailed distribution of NK012, an SN-38-incorporating micelle, in the liver and its potent antitumor effects in mice bearing liver metastases. *Clin Cancer Res* 2010;16:4822–31.
37. Feldman EJ, Lancet JE, Kolitz JE, et al. First-in-man study of CPX-351: a liposomal carrier containing cytarabine and daunorubicin in a fixed 5:1 molar ratio for the treatment of relapsed and refractory acute myeloid leukemia. *J Clin Oncol* 2011;29:979–85.
38. Parhi P, Mohanty C, Sahoo SK. Nanotechnology-based combinational drug delivery: an emerging approach for cancer therapy. *Drug Discov Today* 2012;17:1044–52.

# Cyclic RGD-Linked Polymeric Micelles for Targeted Delivery of Platinum Anticancer Drugs to Glioblastoma through the Blood–Brain Tumor Barrier

Yutaka Miura,[†,‡,§] Tomoya Takenaka,[†] Kazuko Toh,[§] Shourong Wu,[§] Hiroshi Nishihara,[△] Mitsunobu R. Kano,[∥] Yasushi Ino,[⊥] Takahiro Nomoto,[#] Yu Matsumoto,[§] Hiroyuki Koyama,[‡] Horacio Cabral,[#] Nobuhiro Nishiyama,[○,*] and Kazunori Kataoka[†,◇,§,*]

[†]Department of Materials Engineering, Graduate School of Engineering, The University of Tokyo, 7-3-1 Hongo, Bunkyo-ku, Tokyo 113-8656, Japan, [‡]Division of Tissue Engineering, Graduate School of Medicine, The University of Tokyo, 7-3-1 Hongo, Bunkyo-ku, Tokyo 113-8655, Japan, [§]Center for Disease Biology and Integrative Medicine, Graduate School of Medicine, The University of Tokyo, 7-3-1 Hongo, Bunkyo-ku, Tokyo 113-0033, Japan, [△]Department of Translational Pathology, Graduate School of Medicine, Hokkaido University, N15W7, Kita-ku, Sapporo 060-8638, Japan, [∥]Department of Pharmaceutical Biomedicine, Graduate School of Medicine, Dentistry, and Pharmaceutical Science, Okayama University, 1-1-1 Tsushima-naka, Kita-ku, Okayama 700-8530, Japan, [⊥]Division of Innovative Cancer Therapy, The Institute of Medical Science, The University of Tokyo, 4-6-1 Shirokanedai, Minato-ku, Tokyo 108-8639, Japan, [#]Department of Bioengineering, Graduate School of Engineering, The University of Tokyo, 7-3-1 Hongo, Bunkyo-ku, Tokyo 113-8656, Japan, [○]Polymer Chemistry Division, Chemical Resources Laboratory, Tokyo Institute of Technology, R1-11, 4259 Nagatsuta, Midori-ku, Yokohama 226-8503, Japan, and [◇]Center for NanoBio Integration, The University of Tokyo, 7-3-1 Hongo, Bunkyo-ku, Tokyo 113-8656, Japan

**ABSTRACT** Ligand-mediated drug delivery systems have enormous potential for improving the efficacy of cancer treatment. In particular, Arg-Gly-Asp peptides are promising ligand molecules for targeting $\alpha_v\beta_3/\alpha_v\beta_5$ integrins, which are overexpressed in angiogenic sites and tumors, such as intractable human glioblastoma (U87MG). We here achieved highly efficient drug delivery to U87MG tumors by using a platinum anticancer drug-incorporating polymeric micelle (PM) with cyclic Arg-Gly-Asp (cRGD) ligand molecules. Intravital confocal laser scanning microscopy revealed that the cRGD-linked polymeric micelles (cRGD/m) accumulated rapidly and had high permeability from vessels into the tumor parenchyma compared with the PM having nontargeted ligand, "cyclic-Arg-Ala-Asp" (cRAD). As both cRGD/m- and cRAD-linked polymeric micelles have similar characteristics, including their size, surface charge, and the amount of incorporated drugs, it is likely that the selective and accelerated accumulation of cRGD/m into tumors occurred *via* an active internalization pathway, possibly transcytosis, thereby producing significant antitumor effects in an orthotopic mouse model of U87MG human glioblastoma.

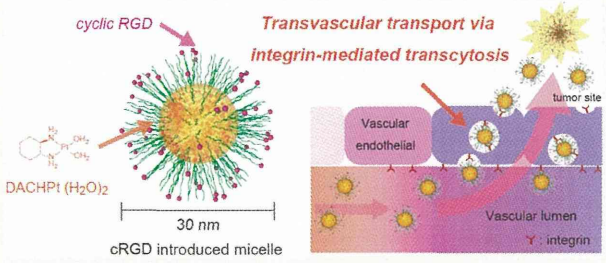


**KEYWORDS:** drug delivery · block copolymer · polymeric micelle · integrin · cRGD · cancer therapy

Treatment of glioblastoma (GBM) is one of the greatest challenges in cancer therapy.[1−4] Although a large number of advanced treatment paradigms have had impacts on medical management for other tumors, prolongation of GBM patients' survival has not been achieved in decades.[5−9] Because of the difficulty of complete surgical excision, irradiation and chemotherapy play important roles in conventional GBM treatment. However, the effects of chemotherapy on GBM are very limited as a result of poor drug penetration from vessels into tumors caused by the vascular/tumor barrier such as the blood–brain barrier (BBB) and the blood–brain tumor barrier (BBTB).[10−15] In fact, the vascular/tumor barrier is highly variable and heterogeneous in the brain. At the early stage of GBM, the tumor cells use the normal brain vessels, which are protected by the BBB, for their growth.[11,13−17] The gradual progression of GBM and its neovascularization compromise the integrity of BBB and lead to the formation of BBTB.[11,16,17] By the time GBM is diagnosed,

* Address correspondence to kataoka@bmw.t.u-tokyo.ac.jp; nishiyama@res.titech.ac.jp.

Received for review May 27, 2013 and accepted September 12, 2013.

**Published online** September 12, 2013
10.1021/nn402662d

the tumor has already developed neovasculature and the BBTB is presented. Therefore, it is important to deliver the effective dose of therapeutic agents into tumor tissues through the BBTB. In the clinic, chemotherapeutic agents may be administrated at high concentrations to circumvent the BBTB,[18] although this strategy is always jeopardized by side effects. Thus, alternative approaches are needed to overcome the BBTB and to transport therapeutic agents efficiently to brain tumors using smart drug delivery systems (DDSs).[19−25]

In general, the main driving force for tumor accumulation of drug carriers can be explained by the enhanced permeability and retention (EPR) effect, which is characterized by microvascular hyperpermeability to circulating macromolecules and impaired lymphatic drainage in tumor tissues.[26] However, the presence of the BBTB limits the EPR effect, thereby resulting in the poor efficacy in drug delivery to GBM.[17,27] A feasible approach for overcoming this issue is the use of ligands that facilitate the translocation of drug carriers across the endothelium of the tumor vasculature. Here, we focused on cyclic Arg-Gly-Asp (cRGD)[25] as a candidate ligand because this cyclic peptide has selective affinity for the $\alpha_v\beta_3$ and $\alpha_v\beta_5$ integrins that are overexpressed on the endothelial cells of tumor angiogenic vessels[28,29] as well as on GBM cells (*e.g.*, the U87MG cell line)[30−32] and because cRGD-linked nanocarriers have shown therapeutic efficacy in GBM.[33,34] However, the mechanisms for the accumulation of cRGD-linked nanocarriers in GBM are still controversial. In this regard, we have recently demonstrated the spatiotemporal and quantitative analyses of extravasation, tissue penetration, and cellular internalization of drug carriers in a living animal through the intravital confocal laser scanning microscopy (IVCLSM) technique.[35−38] Thus, we adapted this technique to long-circulating cRGD-linked nanocarriers for studying the penetration pathway and the derived therapeutic activity of cRGD-mediated DDS. To our knowledge, no systematic research exists addressing the *in situ* observation of translocating behavior of the drug-incorporated cRGD nanocarriers crossing the vascular barrier, and mechanisms involved in cRGD-induced transvascular transport have not been clearly proven yet.

We here developed new long-circulating, cyclic RGD-linked polymeric micelles (PMs) incorporating (1,2-diaminocyclohexane)platinum(II) (DACHPt), the parent complex of the potent anticancer drug oxaliplatin, through the metal complex formation-driven self-assembly of poly(ethylene glycol) (PEG)-*b*-poly(L-glutamic acid) and DACHPt in an aqueous milieu (DACHPt/m).[35,39,40] A series of cRGD-linked DACHPt/m (cRGD/m) was prepared with various cRGD conjugation ratios, ranging from 5% to 40%, in the distal ends of the PEG strands in the outer-shell layer of the PMs. We compared their antitumor effects against GBM with a control DACHPt/m linked with the nontargeted

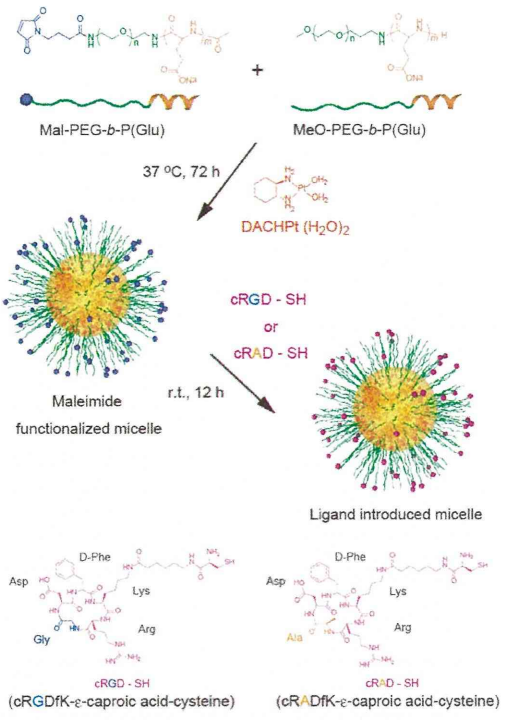


**Figure 1. Schematic showing the design and synthesis strategy for the ligand-linked DACHPt/m.**

peptide cyclic-Arg-Ala-Asp (cRAD). Intravital confocal laser scanning microscopy was used to observe the behaviors of the micelle at tumor sites. This showed that cRGD/m, but not control micelles, could bypass vascular/tumor barriers *in situ* and penetrate deep into GBM through cRGD-induced transvascular transport presumably related to transcytosis, resulting in the induction of potent antitumor effects against malignant glioma.

## RESULTS AND DISCUSSION

**Development of Surface-Tunable DACHPt/m.** cRGD/m with varying densities of cRGD ligand were prepared by "postconjugating" Cys-containing cRGD peptides onto maleimide-functionalized DACHPt/m (the precursor micelle) obtained from a mixture of poly(ethylene glycol)-*b*-poly(L-glutamic acid) (MeO-PEG-*b*-P(Glu)) and maleimide-conjugated poly(ethylene glycol)-*b*-poly(L-glutamic acid) (Mal-PEG-*b*-P(Glu)) (Figure 1). The key features of this strategy are related to the preparation of the precursor micelles, where maleimide functional groups on the micelle surface at a controlled density allow highly reproducible introduction of any ligand molecule with thiol residues. Mal-PEG-*b*-P(Glu) was prepared according to the following scheme. Ring-opening polymerization of the *N*-carboxy anhydride of $\gamma$-benzyl L-glutamate with $NH_2$-PEG-$N_3$ yielded the azido-terminated diblock copolymer $N_3$-poly(ethylene glycol)-*b*-poly($\gamma$-benzyl L-glutamate) ($N_3$-PEG-*b*-PBLG), which was followed by the removal of the $\gamma$-benzyl side chain under